Clays and Clay Minerals, Vol. 58, No. 2, 205–219, 2010.

DOLOCRETES AND ASSOCIATED PALYGORSKITE OCCURRENCES IN SILICICLASTIC RED MUDSTONES OF THE SARIYER FORMATION (MIDDLE MIOCENE), SOUTHEASTERN SIDE OF THE ÇANAKKALE STRAIT, TURKEY

SELAHATTİN KADİR[1,*], MUHSİN EREN[2], AND EŞREF ATABEY[3]

[1] Department of Geological Engineering, Eskişehir Osmangazi University, TR-26480 Eskişehir, Turkey
[2] Department of Geological Engineering, Mersin University, TR-33343 Mersin, Turkey
[3] General Directorate of Mineral Research and Exploration (MTA), TR-06520 Ankara, Turkey

Abstract—The origins of dolocrete and associated palygorskite in the Çanakkale region of Turkey have been little studied, but are of fundamental importance for a more complete understanding of the mineralogy of this region. The present study was undertaken in order to narrow this gap. Siliciclastic red mudstones within alluvial-fan deposits of the Middle Miocene Sarıyer Formation locally contain dolocretes in various forms (powdery, nodular, and fracture-filling) and scarce matte-brown, authigenic clay lenses. The mineralogical characteristics of dolocrete and authigenic clay lenses were examined using polarized-light microscopy, X-ray diffraction, differential thermal analysis and thermal gravimetry, scanning-electron microscopy, and infrared spectroscopy, as well as by chemical and isotopic methods. These analyses indicate that the dolocretes are indeed predominantly dolomite, coexisting with variable amounts of palygorskite. The authigenic clay lenses are composed mainly of palygorskite. Dolomite appears as euhedral crystals, whereas palygorskite developed authigenically as interwoven fibers on and between resorbed dolomite crystals, rimming euhedral crystals, and as fiber bundles (where dolomite ± magnesite is absent). The stable-isotope values and some petrographic features, such as alveolar texture and dolomite needles, support a pedogenic origin for the dolocretes. In the initial stage, dolomite formed by replacement of siliciclastic red mudstones and/or by precipitation from percolating soil-derived water in a near-surface setting. Subsequently, palygorskite either precipitated on the dolomite crystals from relatively more evaporative water, replaced the host-rock mudstone in the presence of Al + Fe, or formed directly from solution where the Ca/Mg ratio decreased and the Al + Fe increased. In view of the large Cr and Ni contents of the bulk-rock samples, the elements required for the crystallization of dolomite and palygorskite (namely Mg, Ca, Si, Al, and Fe) may have been supplied by weathering of ophiolitic rocks that crop out in the area.

Key Words—Dolocrete, Dolomite, Geochemistry, Mineralogy, Palygorskite, Siliciclastic Mudstone, Stable Isotopes, Turkey.

INTRODUCTION

Within-soil and near-surface accumulations of calcite or dolomite are known as calcretes (or caliche) or dolocretes, respectively (Wright and Tucker, 1991). Numerous studies have dealt with various aspects of calcretes in general (*e.g.* Goudie, 1983; Wright and Tucker, 1991; Alonso-Zarza, 2003), calcrete profiles and their origin (*e.g.* Reeves, 1970; Harrison, 1977; Arakel, 1986; Alonso-Zarza and Arenas, 2004; Eren *et al.*, 2008), biogenic features (*e.g.* Klappa, 1980; Jones and Ng, 1988; Wright *et al.*, 1988; Goudie, 1996), chemistry (*e.g.* Aristarain, 1970; Goudie, 1972; Sancho *et al.*, 1992; Khadkikar, 2005), paleoclimate (*e.g.* Mack *et al.*, 1991), associated authigenic clays (*e.g.* Kapur *et al.*, 1987; Verrecchia and Coustumer, 1996; Kadir and Eren, 2008), and morphology (*e.g.* Eren, 2007). In contrast to calcretes, dolocretes have been studied relatively little (*e.g.* Arakel, 1986; Khalaf, 1990, 2007; Colson and Cojan, 1996; Schmid *et al.*, 2006). Two main models have been used to explain the formation of calcrete/dolocrete: (1) the '*per descensum'* model (pedogenic calcrete/dolocrete) based on downward movement of dissolved $CaCO_3$, and (2) the '*per ascensum'* model (groundwater calcrete/dolocrete), related to the capillary rise of groundwater (Goudie 1973, 1983; Wright and Tucker, 1991). The previous studies listed above suggested that dolocretes form from groundwater or surface water by progressive evaporation. Identification of precise sources of Mg is problematic, but it is considered to have been supplied by means of an influx of waters from Mg-rich rocks (Arakel, 1986).

Calcretes in Turkey have been studied by a number of workers (Kapur *et al.*, 1987, 1990, 1993, 2000; Atalay, 1996; Atabey *et al.*, 1998; Eren *et al.*, 2004, 2008; Kadir and Eren, 2008). Eren *et al.* (2004, 2008) provided detailed descriptions of calcretes of the Mersin area and suggested that those calcretes have a pedogenic origin. Furthermore, Kapur *et al.* (1987) and Kadir and Eren (2008) explained the occurrence of palygorskite associated with calcretes in the Adana and Mersin areas, respectively. To date no detailed information has

* E-mail address of corresponding author:
skadir_esogu@yahoo.com
DOI: 10.1346/CCMN.2010.0580206

become available concerning dolocrete in Turkey. The present study focuses on the formation of dolocrete and coexisting palygorskite in the Çanakkale area.

GEOLOGICAL SETTING

Middle to Late Miocene terrestrial and marine sedimentary rocks deposited in the Çanakkale Basin are exposed along the southeastern margin of the Çanakkale Strait (Figures 1, 2). These sedimentary units uncomformably overlie Paleozoic schists and marbles, Permian to Triassic ophiolitic rocks, and Eocene volcanic rocks between Çanakkale and Truva-Küçük Menderes Çay, and only Eocene volcanic rocks crop out in the Lapseki area (Atabey *et al.*, 2004). These sedimentary units comprise the Middle Miocene Sarıyer Formation and the Late Miocene Çanakkale Formation. The Sarıyer Formation is composed of red alluvial-fan deposits, consisting of conglomerate, sandstone, and reddish-gray mudstone in which dolocretes are abundant, and also locally enclose scarce, matte-brown, authigenic clay lenses. The conglomerate is composed of abundant

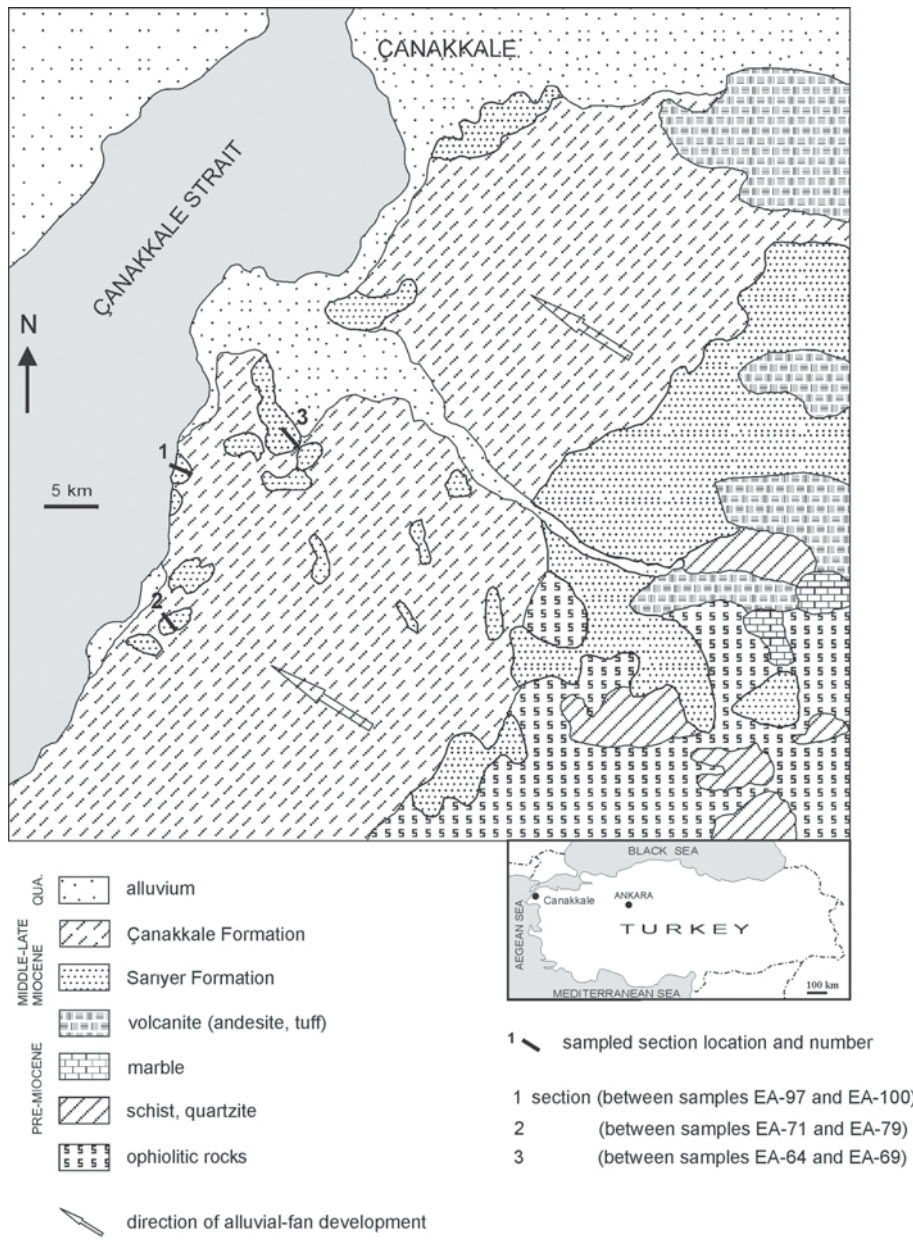

Figure 1. Geological and location maps of the study area.

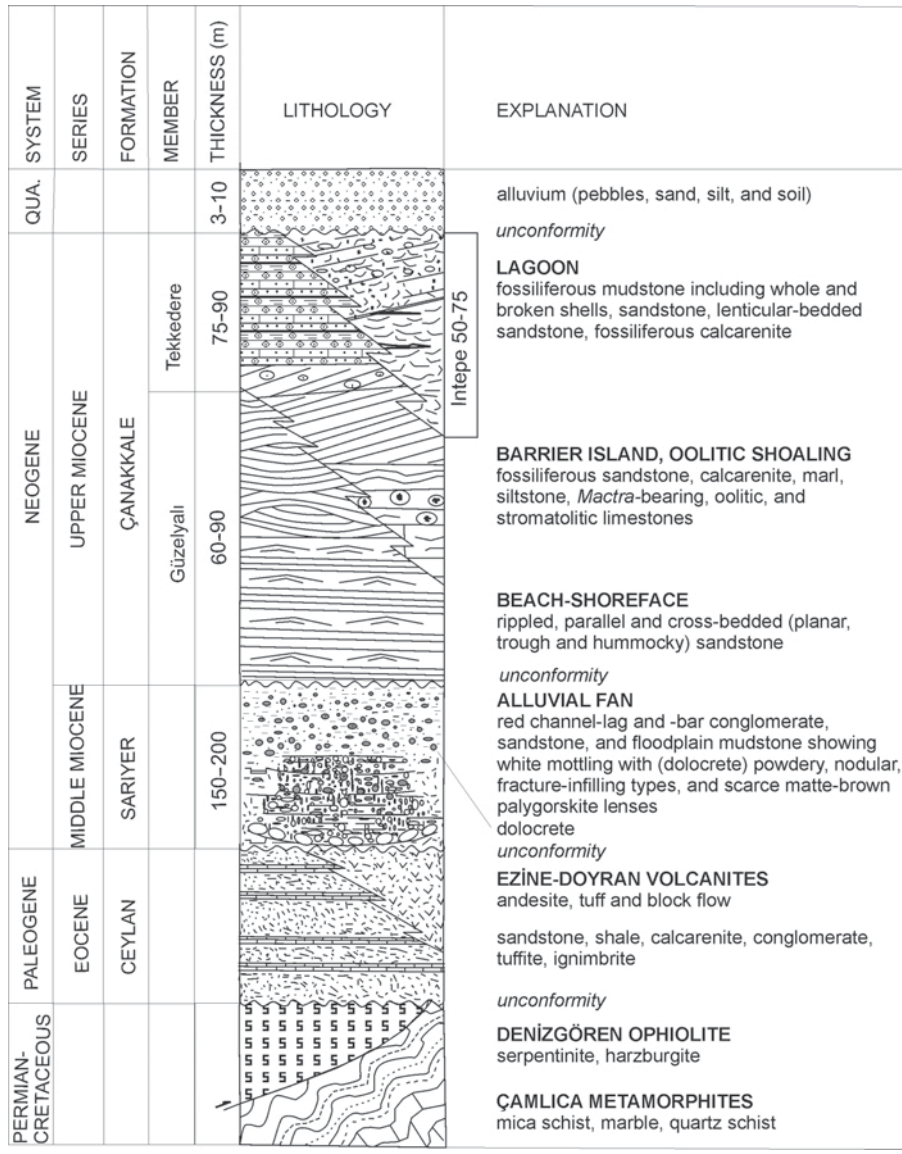

Figure 2. Simplified general stratigraphic section for the study area (modified from Atabey *et al.*, 2004)

serpentinite pebbles, and metamorphic, andesite, and rhyolite pebbles are also present. In the study area, the grain size in the Sarıyer Formation decreases from east to west and northwest where siliciclastic red mudstone dominates (Figure 1). The Çanakkale Formation is subdivided into three members: the Güzelyal, Intepe, and Tekkedere. These members are vertically and laterally gradational. The Güzelyal member comprises fine- to coarse-grained sandstones, mudstone, siltstone, and conglomerate that were deposited in shore and shoreface environments. The Intepe member is composed of mudstone, siltstone, and sandstone deposited as calcarenite and claystone units in a lagoonal environment, on the basis of their fossil contents and sedimentary structures. Mudstone of the Intepe member encloses relict plant stems and alternates with sandstones. The Tekkedere member is composed of algal limestone, oolitic limestone, beach pebblestone, and sandstone, characteristic of deposition in a nearshore environment. The Çanakkale Formation is overlain by Pleistocene marine terraces and Pleistocene–Recent alluvium.

The siliciclastic red mudstones in the alluvial-fan deposits of the Sarıyer formation contain white dolocrete mottlings, with powdery, nodular, and fracture-infilling forms, as well as authigenic clay (palygorskite) lenses. The age of the dolocrete has not been determined. Field observations suggest a relative age younger than Middle

Miocene. Calcretization was a major process during the Pleistocene to Early Holocene (Özer *et al.*, 1989; Atalay, 1996; Kapur *et al.*, 1987, 1990, 2000; Eren *et al.*, 2004, 2008), and the dolocrete of this study may be attributed to the same period of calcretization.

MATERIALS AND METHODS

Twenty-nine samples of dolocrete and material from authigenic clay lenses and their host rocks were collected. Thin sections were prepared from the dolocrete samples and examined using an optical microscope (Nikon-LV 100Pol). The mineralogical characteristics of the samples were determined by X-ray powder diffraction (XRD) (Rigaku Geigerflex), differential thermal analysis-thermal gravimetry (DTA-TG Rigaku TAS 100 E), and scanning electron microscopy (SEM-EDX) (JEOL JSM 84A-EDX). The XRD analyses were performed using CuKα radiation at a scanning speed of 1º2θ/min with tube voltage and current of 40 kV and 30 mA, respectively.

Selected samples were prepared for clay-mineral analysis (size fraction <2 μm) by separation of the clay fraction by sedimentation, followed by centrifugation of the suspension after dispersion overnight in distilled water. The clay particles were dispersed by ultrasonic vibration for ~15 min. Four oriented specimens of the <2 μm fraction of each sample were prepared by either air drying, ethylene-glycol solvation at 60ºC for 2 h, or thermal treatment at 350ºC or 550ºC for 2 h. Semi-quantitative estimates of the rock-forming minerals were obtained by using the external standard method of Brindley (1980), whereas the relative abundances of clay-mineral fractions were determined using basal reflections and the mineral intensity factors of Moore and Reynolds (1989).

Representative clay- and carbonate-dominated bulk samples were prepared for SEM-EDX analysis by adhering the fresh, broken surface of each sample onto an aluminum sample holder with double-sided tape and covering with a thin (350 Å) gold coating using a Giko ion coater. The DTA-TG curves were recorded using 10 mg of powdered sample in a Pt sample holder at an average rate of 10ºC/min with an alumina reference. Infrared (IR) spectroscopic analysis was performed on pressed pellets of powdered clay samples (2 mg of

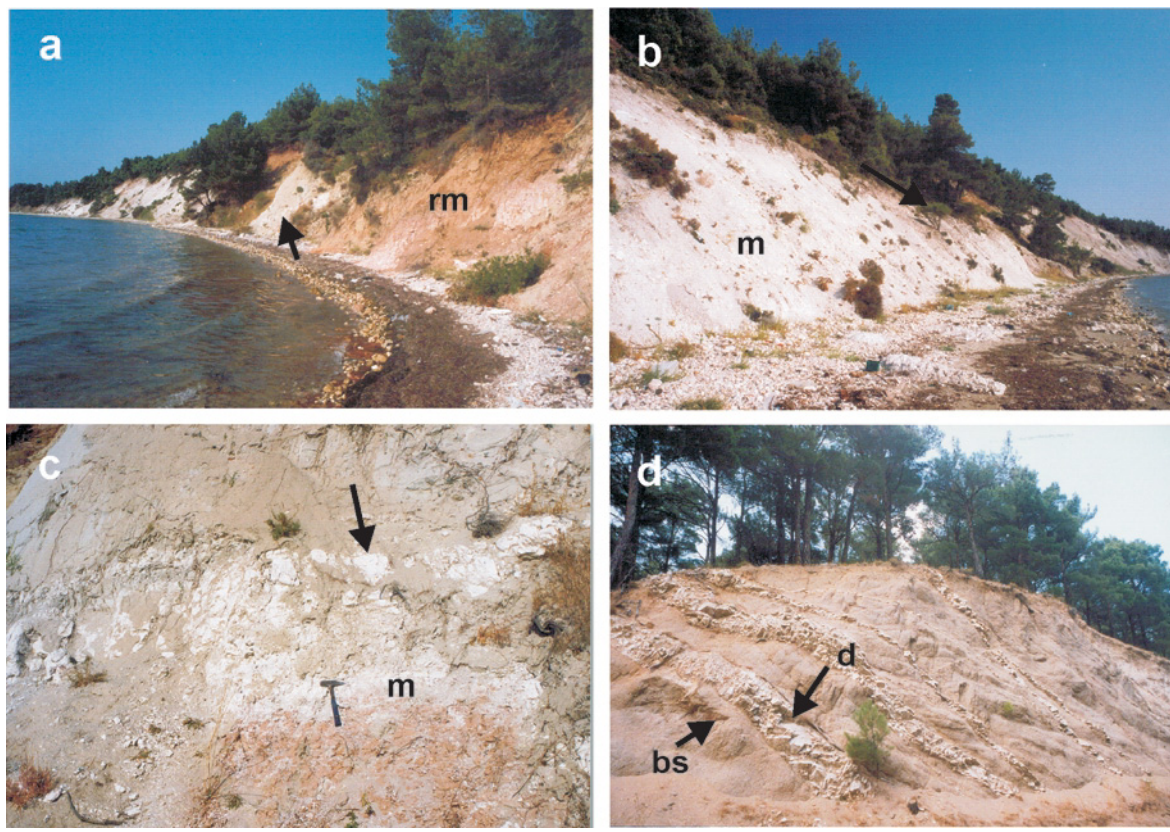

Figure 3. Field photographs showing dolocrete occurrences in siliciclastic mudstones of the Sarıyer Formation (Middle Miocene) along the Çanakkale Strait: (a) white dolocrete mottlings (arrows) in the red mudstone (rm); (b) close-up view of dolocrete mottling (m); (c) fracture-controlled dolocrete nodules (arrow) and powdery dolocrete (m); (d) dolocrete as a fracture-filling (d), cross-cutting the bedding surface (bs) and decreasing downward.

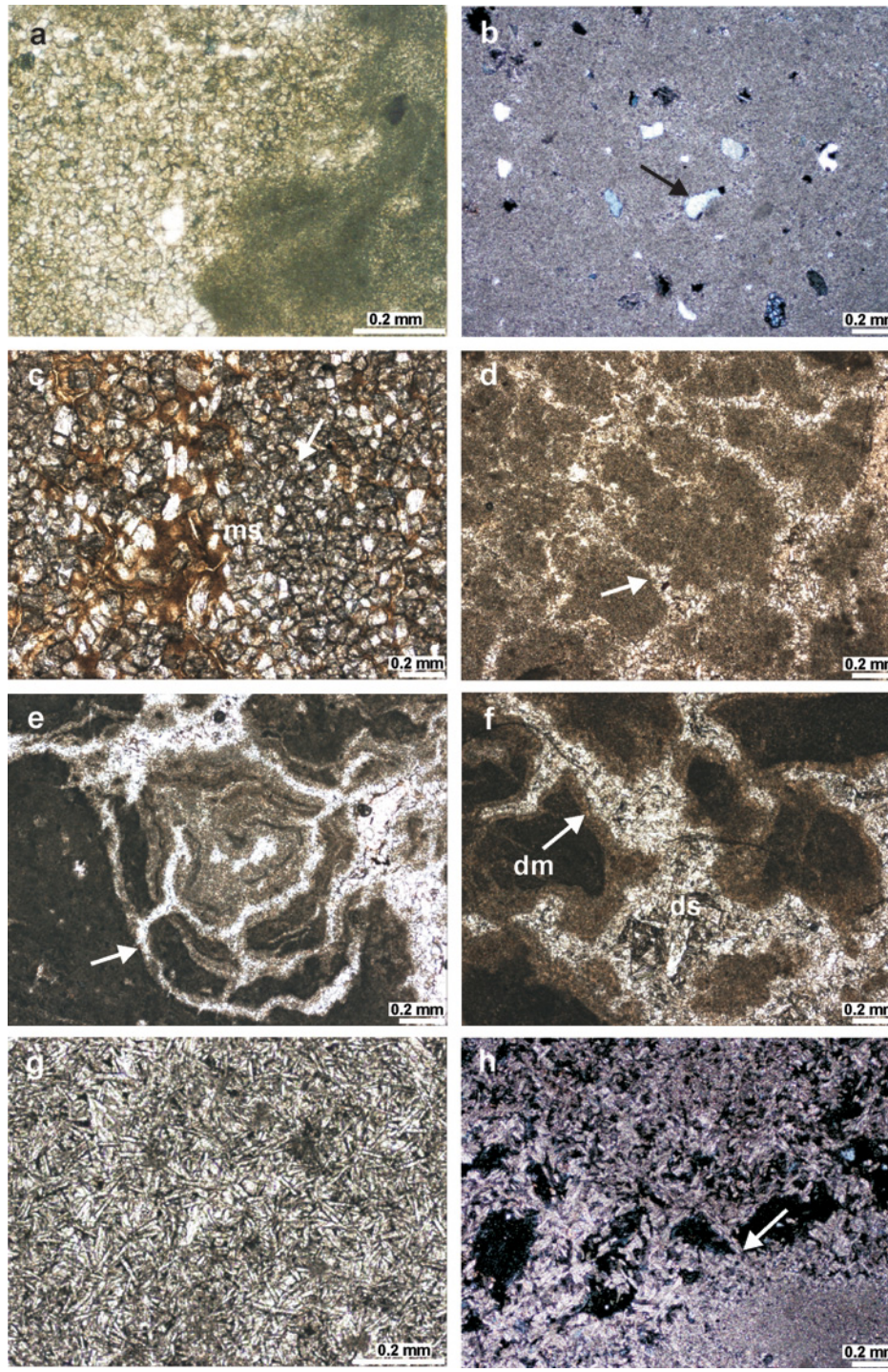

Figure 4. Dolocrete photomicrographs: (a) very finely to finely crystalline dolomite showing recrystallization from dolomicrite (dark areas) to dolomicrosparite, ppl (EA-93), scale bar = 0.2 mm; (b) floating texture, displaying detrital quartz grains (arrow) in dolomicritic groundmass, xpl (EA-99); (c) sparry dolomite including clay-infilling (brown) in intercrystalline pores, ppl (EA-78B); (d) desiccation cracks (arrow) with sparry dolomite filling in groundmass of very finely crystalline dolomicrosparite, ppl (EA-72); (e) curvilinear desiccation cracks (arrow) with sparry dolomite filling, ppl (EA-72); (f) vuggy pore showing very finely crystalline dolomicrosparitic rim cement (arrow) and sparry-dolomite cement (ds) at the pore center, dm: dolomicrite, ppl (EA-74); (g) acicular dolomite crystals forming a mesh-like structure, ppl (EA-73); (h) acicular, oriented, or suboriented dolomite crystals (arrow) forming pore walls with alveolar texture, xpl (EA-73). ppl: plane-polarized light; xpl: crossed polars.

<2 μm fraction) mixed with 200 mg of KBr using a Perkin Elmer 100 FT-IR spectrometer; scans were made at a 4 cm^{-1} resolution.

Chemical data for 16 representative samples of dolocrete and their host rocks were obtained by X-ray fluorescence (XRF) (Rigaku RIX 3000 X-ray fluorescence spectrometer). Chemical analyses were performed using the rock standards of the MBH Reference Material (1998-99) and Breitländer (1988). The detection limits for the analyses were between 0.01 and 0.1 wt.% for major elements and 10 ppm for trace elements.

Loss on ignition (LOI) for each sample was also determined by drying the samples overnight at 105ºC, followed by determination of their water contents (and the contents of other volatiles) at 1050ºC. Carbon and oxygen isotopes were determined using a Finigan MAT 252 mass spectrometer in the laboratories of Southern Methodist University (SMU), Dallas, Texas (USA). Powdered calcrete samples (510 mg) were reacted with 100% phosphoric acid (H_3PO_4) at 50ºC. Replicate analyses on randomly selected samples gave a mean deviation of ±0.05‰ for oxygen and ±0.02‰ for carbon. All isotopic data are reported in per mil (‰) with respect to the PDB standard.

RESULTS

Field descriptions

In the field, the dolocretes and scarce authigenic clay lenses appear as white (Figure 3) and matte-brown mottlings, respectively, in siliciclastic red mudstones of the Middle Miocene Sarıyer formation. The dolocrete mottlings are discontinuous and occur as powdery, nodular, and fracture-filling forms. The powdery and nodular dolocretes are irregular in shape (Figure 3a–c) and are often controlled by non-tectonic fractures (Figure 3c). The fracture-filling dolocretes are elongated (Figure 3d), cross-cut bedding, and decrease downward.

Petrography

Petrographic examination of thin sections indicated that the dolocrete samples are predominantly very fine-

Table 1. Semi-quantitative mineralogical compositions of the dolocretes, authigenic clay lenses, and host-rock samples.

Sample	Rock type	pal	smc	chl	ill	dol	mag	cal	qtz	fds	pyx	talc
EA-66	dolocrete powder	++	+			++						
EA-67	dolocrete powder	+++	acc			++						
EA-69	dolocrete powder	++				+++			acc			
EA-78B	dolocrete powder	+++				++			acc			
EA-97	dolocrete powder	+++		acc			++		acc			acc
EA-94	dolocrete powder	++				+++						
EA-95	dolocrete powder	++	acc			+++						
EA-98	dolocrete powder	++				+++			acc			
EA-65	dolocrete nodule	+	acc			+++++						
EA-70	dolocrete nodule	+				++	+					
EA-72	dolocrete nodule	+				++++						
EA-73	dolocrete nodule	+				++++						
EA-74	dolocrete nodule	+				++++			acc			
EA-75	dolocrete nodule	+				++++						
EA-76	dolocrete nodule	+				++++						
EA-77	dolocrete nodule	+	acc			++++						
EA-79	dolocrete nodule	+				++++						
EA-93	dolocrete nodule	acc				+	+++					
EA-96AB	dolocrete nodule	+	+	+		++	+		acc			acc
EA-99	dolocrete nodule	+	acc			+++			acc			
EA-68	dolocrete fracture-filling	++				+++			acc			
EA-64	clay lens	+++++				+			acc			
EA-71	clay lens	+++++				acc			acc			
EA-100	clay lens	+++++	acc	acc					acc			
EA-118	mudstone	+	+	+					++	acc		
EA-119	mudstone	+++		acc	acc					+	acc	
EA-120	mudstone		+		acc	+		+	++	acc		
EA-121	mudstone	acc	++	acc					+	++		
C-5	mudstone		++++		acc				+		acc	
C-11A	mudstone		++++		acc				acc		+	
C-12	mudstone		++		+	+			acc	+		

pal: palygorskite, smc: smectite, chl: chlorite, ill: illite, dol: dolomite, mag: magnesite, cal: calcite, qtz: quartz, fds: feldspar, pyx: pyroxene.

grained crystalline dolomicrosparite and dolomicrite (Figure 4a,b); patchy dolospar (Figure 4c) is also present as a product of recrystallization. Desiccation cracks are widespread, with crumbly, polygonal, and curved aspects (Figure 4d–f), accompanied by dolomicrospar infilling. Intensely fractured areas were subjected to recrystallization resulting in dolomicrospar formation. Detrital quartz grains (<5% volume) are present in some samples where they appear to be floating in the groundmass (Figure 4b); this sort of floating texture is characteristic of calcretes (Wright and Tucker, 1991). In thin section, birds-eye fillings and vuggy pores occur locally. The pores are surrounded by rim cement – either scalenohedral or cloudy microcrystalline dolomite, which grades poreward into euhedral sparry dolomite. In sample EA-76, acicular dolomite crystals (17–61 μm) are widespread and form a mesh-like structure (Figure 4g) and/or alveolar texture (Figure 4h) in which voids are surrounded by bundles of parallel or subparallel dolomite needles. Randomly oriented dolomite needles are also present in the pores. Brecciation in some clay-rich samples is also present.

XRD

The mineralogical compositions of bulk samples, the clay fractions of dolocrete nodules, powders, and fracture-fillings, and samples from matte-brown authigenic clay lenses and reddish, greenish, and multicolored siliciclastic mudstone host rocks were examined by XRD (Table 1, Figures 5, 6). The results indicated that dolomite predominates in the samples and is associated locally with accessory magnesite and with abundant palygorskite in powdery and nodular dolocrete samples. The amount of palygorskite increases and dolomite decreases in powdery dolocrete compared to nodular dolocrete. Accessory smectite, chlorite, quartz, pyroxene, illite, and talc are also present in the samples. Matte-brown clay lenses are composed predominantly of palygorskite.

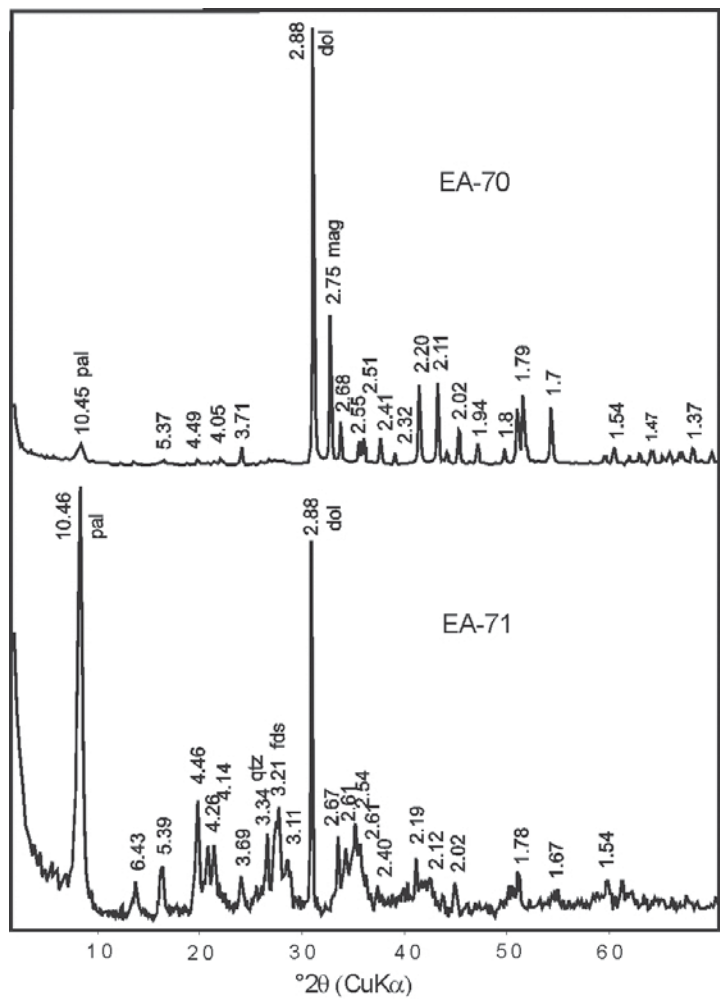

Figure 5. XRD patterns for bulk argillaceous dolocrete. pal: palygorskite, dol: dolomite, mag: magnesite, qtz: quartz, and fds: feldspar.

Host-rock samples comprise smectite, palygorskite, chlorite, quartz, feldspar, illite, and, locally, dolomite and calcite. Thus, palygorskite is either lacking or occurs as an accessory phase in siliciclastic mudstone samples, whereas feldspar and smectite + chlorite + illite are associated with quartz and, locally, with dolomite and calcite.

Palygorskite has sharp diagnostic basal reflections at 10.45 Å which were unaffected by ethylene-glycol treatment, but reduced and then collapsed upon heating at 350 and 550ºC, respectively (Figure 6). Smectite was recognized by its 14.4 Å reflections which expanded to 16.8 Å with ethylene-glycol treatment, and then collapsed to 10.0 and 9.97 Å after heating at 350ºC and 550ºC, respectively, for 2 h (Figure 6). Chlorite was determined from its 14.2, 7.1, and 3.54 Å reflections, and by the fact that it was not affected by ethylene-glycol treatment and heating at 550ºC.

DTA-TG analysis

The DTA-TG analysis of palygorskite-dominated samples showed that sample EA-100 gives four main endothermic peaks at 154ºC (weight loss: 8.8%), 288ºC (weight loss: 3.7%), 473ºC (weight loss: 4.2%), and

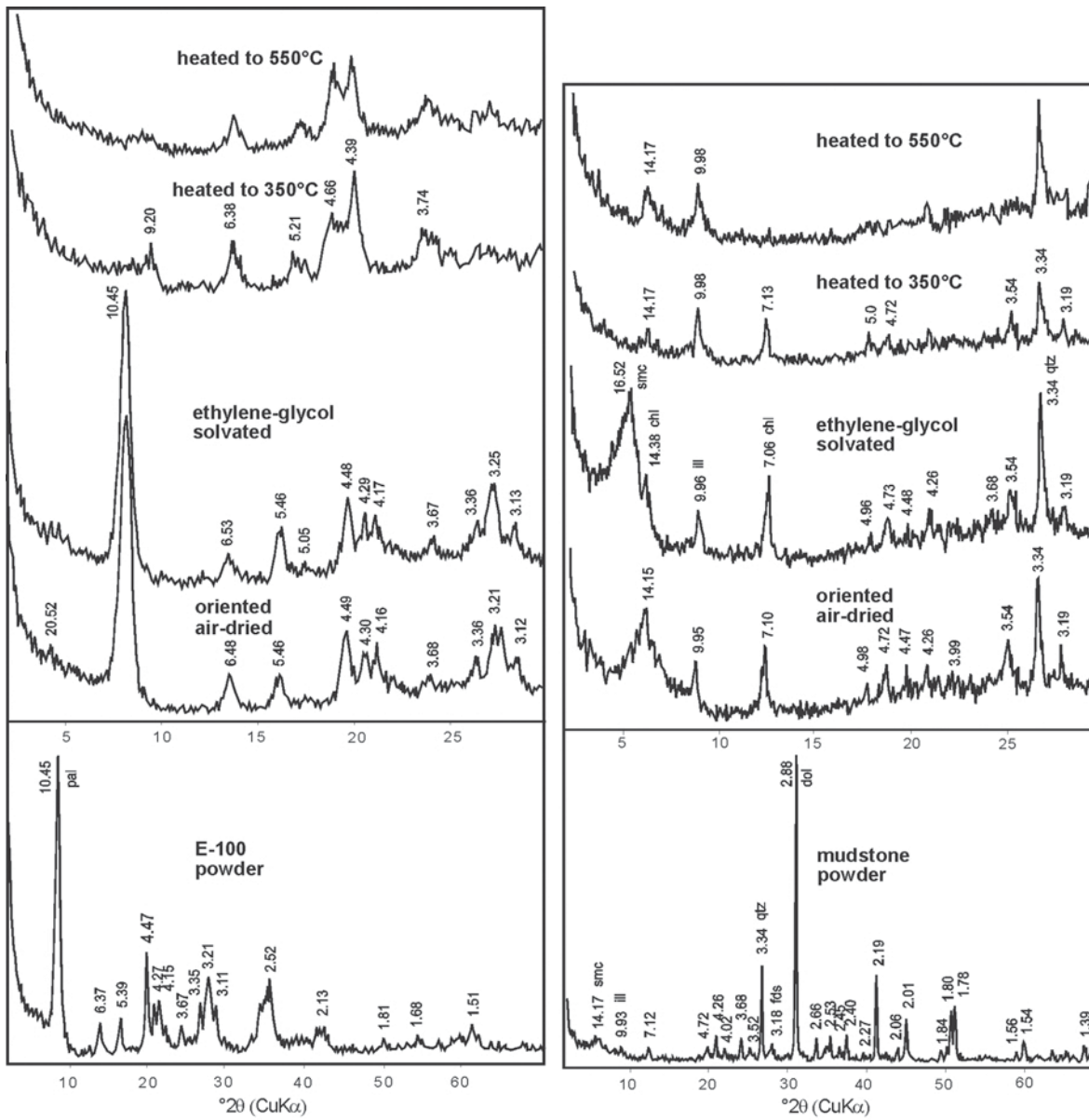

Figure 6. XRD patterns for clay fractions. pal: palygorskite, smc: smectite, chl: chlorite, ill: illite, dol: dolomite, qtz: quartz, fds: feldspar.

800ºC (weight loss: 1.2%) (Figure 7). The first endothermic peak corresponds to the loss of adsorbed and zeolitic water. The second endothermic peak, possibly tied to bound water, is strongly coordinated with Mg atoms within the palygorskite channels, and that water remains stable until it is expelled at the third endothermic peak at 473ºC. The fourth endothermic peak, at ~800ºC, is due to structural dehydroxylation. The last endothermic peak is followed by a weak, broad exothermic peak that is due to the collapse of palygorskite structure, as reported by Kulbicki (1959), Imai *et al.* (1969), and Jones and Galán (1988).

The DTA-TG curve for sample EA-75 has large endothermic peaks at 780ºC (weight loss: 20.3%) and 900ºC (weight loss: 21.4%) due to decomposition of $MgCO_3$ and $CaCO_3$, respectively, in the dolomite structure (Figure 7; Mackenzie, 1957; Webb and Kruger, 1970; Smykatz-Kloss, 1974).

SEM-EDX analysis

The SEM images indicated that dolomite ± accessory magnesite rhombs are dominant in dolocrete samples, coexisting with palygorskite. The dolocrete samples consist of euhedral or subhedral dolomite and accessory magnesite crystals 3–18 μm in maximum dimension. Palygorskite occurs as dense fiber masses and interwoven fibers grown as bridges in resorbed-crystal voids and between relics of dolomite-dominated carbonate crystals (Figure 8a–e). On the other hand, in sample EA-100, taken from an authigenic clay lens, dense palygorskite fibers developed sub-parallel to each other where carbonate crystals are either absent or occur as accessories (Figure 8f–g). Palygorskite also occurs in highly degraded alluvial detritus of the study area (Figure 8h–i).

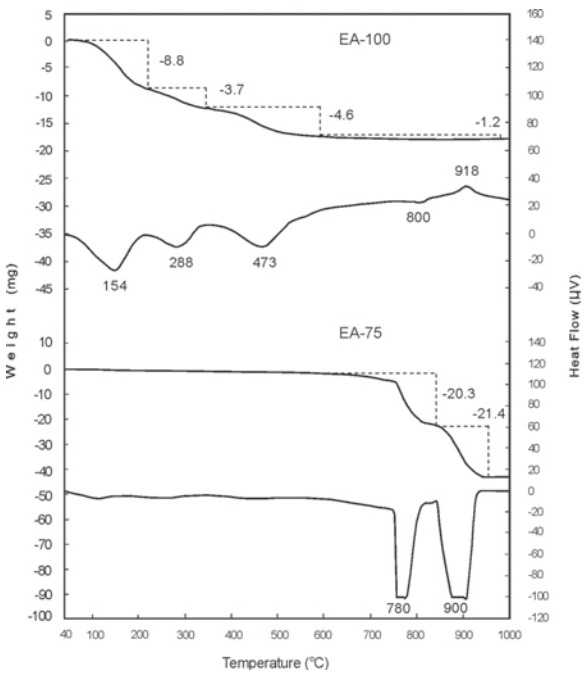

Figure 7. DTA-TG curves for palygorskite and dolomite (EA-100 and EA-75).

Rhombic carbonate crystals show strong peaks for either Ca and Mg, or Mg, suggesting a dolomitic or magnesitic composition. Fibrous palygorskite is indicated by strong Si, moderate Al, and smaller Mg and Fe peaks (Figure 9).

IR spectroscopy

The IR spectra for palygorskite-dominated sample EA-100 and dolomite-dominated EA-75 sample (Figure 10) revealed bands at 3551, 3405, 1662, 988, 648, 583, 511, and 487 cm^{-1}, suggesting the presence of palygorskite. The 3405 cm^{-1} band may be due in part to a large Mg content, which adds Fe-OH-Mg vibrations to the Fe-OH-Al vibrations. The band at 1662 cm^{-1} corresponds to the bending vibrations of bound water and structural hydroxyls, rather than to adsorbed and zeolitic water, which were eliminated upon heating to 105ºC/4 h (Farmer, 1974; Van der Marel and Beutelspacher, 1976; Imai *et al.*, 1969). The 988, 697, and 474 cm^{-1} bands are probably due to the (Mg, Al)–Si–O and Si–O–Si (Al) stretching vibration of palygorskite (Farmer and Russell, 1964; McKeown *et al.*, 2002). Bands at 648, 583, 511, and 487 cm^{-1} are attributed to O–Si–O bending vibrations. Bands at 648 and 511 cm^{-1} may also be attributed to the Mg–O vibration.

The IR spectra for the dolomite-dominated sample EA-75 are characterized by a broad, intense band at 1436 cm^{-1}, and sharp bands at 881 and 729 cm^{-1}, all related to CO_3^{2-} anions (Van der Marel and Beutelspacher, 1976). The IR spectra results were consistent with the results of XRD, SEM, DTA-TG, and chemical analyses of the samples.

Chemical analysis

The results of chemical analyses of palygorskite-bearing dolocrete and palygorskite samples and their reddish, greenish, and multicolored mudstone host rocks are given in Table 2. An increase in loss on ignition values, associated with an increase in CaO + MgO and MgO, is important as an indicator of dolomite ± trace magnesite.

The chemical variations reflect the mineralogies and crystal chemistries of the dolomite minerals that coexist with the clay and detrital minerals (Tables 1 and 2). SiO_2, Al_2O_3, and MgO are abundant in the dolocrete samples, corresponding to an abundance of palygorskite associated with dolomite. Thus, SiO_2, MgO, and loss on ignition increase in the carbonate nodules where the detrital component is absent. The $Al_2O_3 + Fe_2O_3$ contents increase with an increase in palygorskite ± smectite ± chlorite or SiO_2 and MgO, indicating that $Al_2O_3 + Fe_2O_3$ is bound

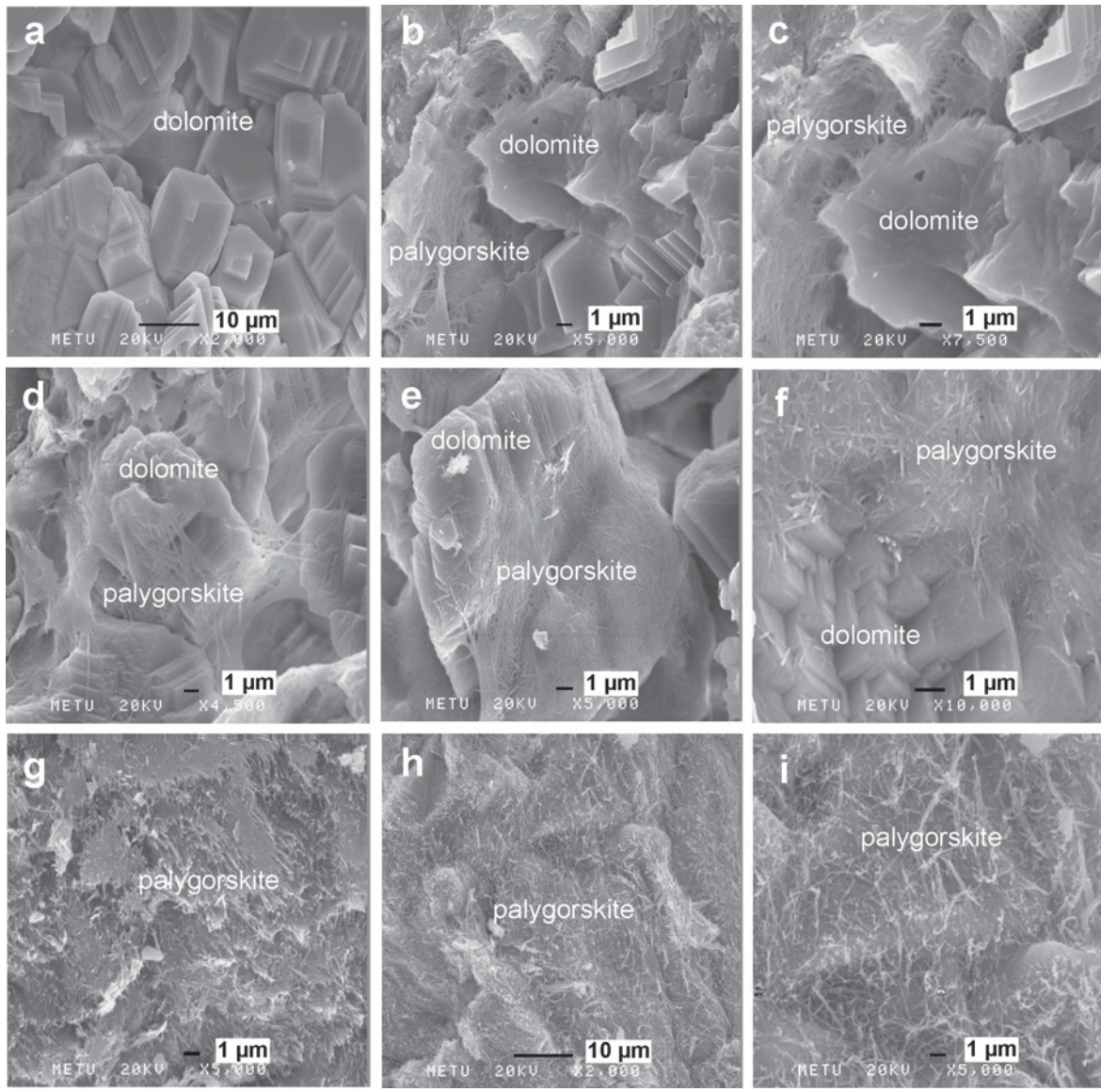

Figure 8. SEM images of: (a) euhedral dolomite crystals (EA-64); (b) palygorskite fibers as bridges between resorbed dolomite crystals (EA-64); (c) close-up view of b; (d–e) interwoven palygorskite fibers in dissolution voids and as bridges between resorbed dolomite crystals (EA-64); (f) palygorskite fiber masses in contact with dolomite rhombs (EA-64); (g) subparallel orientation of palygorskite fibers in a brown clay lens (EA-100); (h–i) dense fibers and interwoven palygorskite development within altered detrital sediments in alluvial-fan materials (multicolored mudstone – alluvial sediments) (EA-119).

within the structures of these minerals, as indicated by mineralogical determinations. The presence of CaO (11.6–29.8%) associated with MgO (12.8–19.5%) reflects the presence of dolomite accompanied by clay minerals. Thus, CaO reflects the presence of dolomite. Palygorskite-rich, brown clay sample EA-100 is composed of 58.4% SiO_2, Al_2O_3 + Fe_2O_3 (11.0% and 6.2%, respectively), 9.0% MgO, and 12.7% LOI.

Cr (952–2023 ppm), Co (50–69 ppm), Ni (702–1444 ppm), Cu (30–50 ppm), and Pb (22–36 ppm) in palygorskite-rich samples (EA-71 and EA-100) correlate positively with Fe_2O_3 + MgO, reflecting the availability of ferromagnesian material which probably originated from serpentinized ophiolitic-basement units.

Stable isotopes

Stable-isotope, $\delta^{18}O$ and $\delta^{13}C$, values for selected dolocrete samples (Table 3) revealed that the dolomite ranged from −2.88 to −5.81 (mean = −4.27) and from −5.59 to −6.77 (mean = −6.43)‰ PDB, respectively. The dolocrete $\delta^{18}O$ values were more variable than their $\delta^{13}C$ values. Considering the oxygen-isotope fractionation value

Table 2. Major- and trace-element compositions of dolocretes, authigenic clay lenses, and host-rock samples.

	Dolocrete								Authigenic clay lenses			– Mudstone (host rock) –		
Oxide (%)	EA-65	EA-66	EA-67	EA-68	EA-69	EA-72	EA-77	EA-78B	EA-79	EA-99	EA-64	EA-71	EA-100	EA-118	C-5	C-11A
SiO_2	5.9	19.5	22.5	18.5	10.6	2.1	7.0	7.0	4.0	8.2	39.0	51.5	58.4	66.3	54.3	46.2
Al_2O_3	1.7	4.8	3.4	3.1	1.6	0.3	1.2	1.2	0.8	1.0	7.5	8.3	11.0	14.0	17.0	23.0
Fe_2O_3	0.7	2.1	1.5	1.3	0.7	0.1	0.9	1.0	0.4	0.6	3.5	10.5	6.2	0.5	10.5	9.5
MgO	18.5	16.5	17.6	17.5	18.2	19.5	18.5	18.8	19.0	18.5	12.8	9.5	9.0	0.1	4.0	2.0
CaO	28.5	21.0	20.0	24.5	26.5	31.6	28.2	28.5	29.8	27.8	11.6	2.4	0.2	0.3	1.7	1.8
Na_2O	0.1	0.1	0.1	0.1	0.1	0.1	0.1	0.1	0.1	0.1	0.1	0.1	0.1	1.5	1.1	0.7
K_2O	0.2	0.6	0.2	0.3	0.1	0.1	0.1	0.1	0.1	0.1	0.8	0.6	0.6	0.8	1.1	0.4
TiO_2	0.1	0.3	0.2	0.2	0.1	0.1	0.1	0.1	0.1	0.1	0.4	0.7	0.6	0.2	1.1	1.4
MnO	0.1	0.1	0.1	0.1	0.1	0.1	0.1	0.1	0.1	0.1	0.1	0.1	0.1	0.1	0.1	0.1
LOI	42.6	35.0	34.5	31.8	41.0	45.8	43.9	42.8	44.9	42.5	22.4	14.1	12.7	15.4	8.1	13.2
Total	98.4	100.0	100.1	97.4	99.0	99.8	100.1	99.7	99.3	98.9	98.2	97.8	98.9	99.2	99.0	98.3
Trace elements (ppm)																
Cr	50	66	50	50	50	50	96	96	50	71	142	2023	952	137	50	50
Co	50	50	50	50	50	50	50	50	50	50	50	69	50	50	50	50
Ni	30	92	75	50	40	72	176	177	85	114	138	1444	702	34	30	30
Cu	30	30	30	30	30	30	30	30	30	30	39	50	30	30	30	94
Pb	20	20	20	20	20	20	20	20	20	20	20	36	22	118	20	20

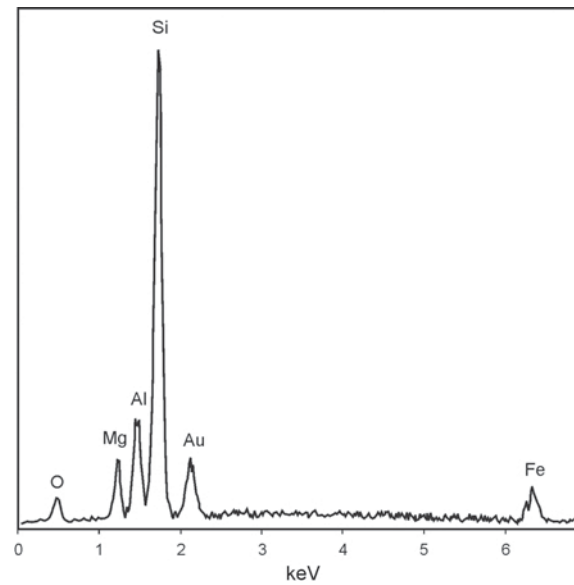

Figure 9. EDX pattern for palygorskite fibers (EA-100).

of 3±1‰ PDB between dolomite and calcite (Land, 1980), the present values are clearly consistent with calcrete (calcite) isotope values (Suchecki *et al.*, 1988; Alonso-Zarza and Arenas, 2004; Bajnoczi and Kovacs-Kis, 2006; Eren *et al.*, 2008). The dolocrete values tend to be enriched in $\delta^{18}O$ and $\delta^{13}C$ relative to those of the calcretes.

DISCUSSION

In the field, dolocrete mottlings occur in near-surface settings within the siliciclastic mudstones and decrease downward, especially in fractures, suggesting formation from percolating water in a near-surface setting. Petrographic features such as desiccation cracks, scarce alveolar texture, and floating grains are characteristics of calcretes/dolocretes, and confirm a near-surface setting or vadose environment (Wright and Tucker, 1991). The

Table 3. Stable-isotope compositions of dolomite in dolocretes.

Sample	$\delta^{18}O$ (PDB)	$\delta^{13}C$ (PDB)
EA-70	−4.23	−6.74
EA-72	−4.31	−6.72
EA-73	−5.43	−6.23
	−5.40	−6.21
EA-74	−3.61	−6.62
EA-75	−4.77	−6.19
EA-76	−5.81	−6.33
	−5.78	−6.32
EA-77	−4.24	−6.74
EA-79	−2.88	−5.59
EA-93	−3.19	−6.77

>

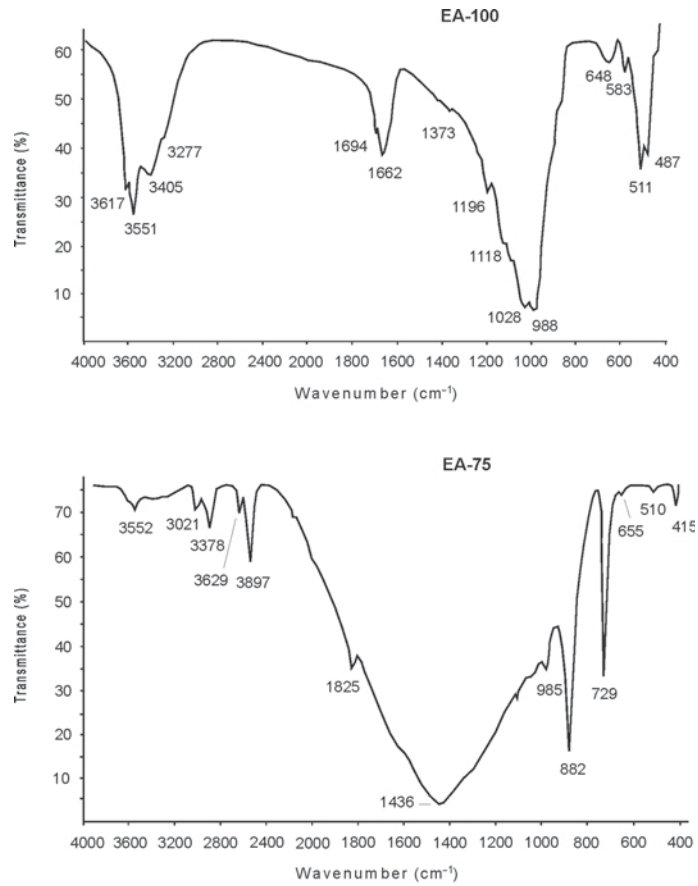

Figure 10. IR spectra for palygorskite (EA-100) and dolomite (EA-75).

oxygen-isotope values indicate formation from meteoric water (James and Choquette, 1984), and the carbon-isotope values suggest a large input of soil-derived carbon (Goudie 1983; Cerling 1984; Purvis and Wright, 1991; Alonso-Zarza and Arenas, 2004). Both negative $\delta^{13}C$ values and alveolar texture in some samples suggest a pedogenic origin for dolocretes in the region (Wright and Tucker 1991; Eren *et al.* 2008). Similar to calcite needles, dolomites needles are interpreted to be a result of fungal biomineralization (Wright, 1986 for calcite needles) and support a pedogenic origin for these dolocretes.

The dominance of micrite in the dolocrete samples suggests rapid precipitation or replacement from a supersaturated solution, followed by extreme super-saturation and slower precipitation of sparitic dolomite during dolocretization (Harrison, 1977; Braithwaite, 1979). The Mg required for the formation of dolocretes was probably supplied by proximal serpentinized ophiolitic-basement units in light of the high Cr and Ni contents of the bulk samples.

Mineralogical and geochemical determinations on dolocrete samples reveal that palygorskite coexisted with dolomite in variable amounts, mainly as a minor component. Determinations by XRD revealed that the sharp diagnostic basal reflection at 10.45 Å is consistent with palygorskites from Sapillo, New Mexico, No. 21 (Christ *et al.*, 1969) and Attapulgus, Georgia (Bradley, 1940). The sharp 3551 and 3405 cm^{-1} bands in IR spectra for palygorskite-rich sample E-100 were attributed to the stretching vibration of hydroxyl groups; the bonding of hydrogen-coordinated Al and Si atoms reveal typical palygorskite, similar to that reported by Serratosa (1962), Farmer and Palmieri (1975), and Van der Marel and Beutelspacher (1976). Examinations by SEM revealed that palygorskite developed either as dense fiber masses and interwoven fibers or bridges on and between resorbed dolomite rhombs in dolocrete samples; the textures suggest that the palygorskite had an authigenic origin. Palygorskite formation post-dated dolomite formation and developed *via* a dissolution-precipitation mechanism; alternatively, masses of palygorskite fibers edging well crystallized rhombic carbonate may reveal direct precipitation following precipitation of carbonate under semi-arid to arid climatic conditions (Singer, 1979, 1989; Jones and Galán, 1988; Inglès and Anadón, 1991; Kadir, 2007; Gürel, 2008). Elsewhere, the subparallel orientation of palygorskite fibers in brown clay lenses

(sample EA-100) may indicate formation by replacement of host-rock mudstones, as well as by precipitation. Locations lacking carbonate crystals are similar to occurrences described by Allison and Riggs (1994), Gehring *et al.* (1995), Akbulut and Kadir (2003), and Kadir and Eren (2008). The chemical contents (58.4% SiO_2, 11.0% Al_2O_3, 6.2% Fe_2O_3, and 9.0% MgO) of palygorskite-rich sample E-100 and its microchemical analysis by EDX (Figure 9) indicated typical palygorskite, similar to palygorskite from Mt. Flinders, Queensland, Australia (Roger *et al.*, 1964), and Barton, Florida, USA (Krekeler *et al.*, 2008), except that it contains more Al_2O_3 + Fe_2O_3 and less MgO (Newman and Brown, 1987). Si and Al + Fe for the formation of palygorskite originated either from the weathering of ophiolitic rocks, (based on large Cr and Ni values in palygorskite-rich samples [*e.g.* EA-100 and EA-71] from dolocrete-bearing mudstone [containing 952 and 2023 ppm Cr, and 702 and 1444 ppm Ni, respectively]), or by degradation of unstable detrital smectite, chlorite, illite, and other sediments (host rocks) which show high degrees of degradation (Tables 2, 3; Velde, 1977). Development of palygorskite between degraded phyllosilicate-dominated detrital materials in the host rock (mudstone) revealed that these phyllosilicates were unstable in a highly alkaline environment, resulting in the release of Si and Al + Fe (Singer, 1984; Paquet, 1983; Chamley, 1989; Çağatay, 1990). Ece *et al.* (1999) reported contents of 23.7% MgO, 7.64% FeO, and 8.24% CaO in Permian to Triassic ophiolitic rocks of the Çanakkale area. Thus, this palygorskite apparently formed in association with smectite- and chlorite-rich, shore and nearshore, alluvial-fan sediments. The Mg necessary for precipitation of palygorskite associated with these dolocretes may also have been supplied by resorption of dolomite and magnesite crystals (*e.g.* Ghazban *et al.*, 1994).

Overall, the dolocretes of the Çanakkale area are of pedogenic origin, probably developed below the vegetation cover from percolating soil-derived water. In that alternating wet and dry periods are known to be important in calcrete/dolocrete formation (Wright and Tucker, 1991), wet periods in the study area presumably caused weathering of ophiolitic rocks and soil formation. Subsequent dry periods increased Mg and Ca concentrations in soil-derived water from which dolomite precipitated and/or replaced the host rocks in an earlier stage; palygorskite later formed in a more evaporative stage.

CONCLUSIONS

In the Çanakkale area, siliciclastic red mudstones in alluvial-fan deposits of the Sarıyer Formation locally contain white dolocrete mottlings and scarce palygorskite lenses along the Çanakkale Strait. Analyses suggest that dolocrete samples are predominantly dolomite with variable amounts of palygorskite. Field and petrographic features and stable-isotope values suggest formation from soil-derived percolating meteoric water in a near-surface setting below the soil zone. A process of progressive drying resulted in dolomite formation by replacement and/or precipitation in an early stage, with palygorskite precipitating in a later stage.

ACKNOWLEDGMENTS

The authors are indebted to anonymous reviewers for careful and constructive reviews, which significantly improved the quality of the paper. They are also grateful to Professor Hailiang Dong (Miami University, Oxford, Ohio) and Professor Joseph W. Stucki (University of Illinois, USA) for their insightful editorial comments and suggestions. The authors are grateful to the General Directorate of Mineral Research and Exploration of Turkey (MTA) for conducting some of the mineralogical analyses.

REFERENCES

Akbulut, A. and Kadir, S. (2003) The geology and origin of sepiolite, palygorskite and saponite in Neogene lacustrine sediments of the Serinhisar-Acpayam basin, Denizli, SW Turkey. *Clays and Clay Minerals*, **51**, 279–292.

Allison, M.A. and Riggs, S.R. (1994) Clay-mineral suites in cyclic Miocene sediments; a model for continental-margin deposition in a mixed siliciclastic-phosphatic-dolomitic-biogenic system. *Journal of Sedimentary Research*, **64**, 386–395.

Alonso-Zarza, A.M. (2003) Palaeoenvironmental significance of palustrine carbonates and calcretes in the geological record. *Earth Science Reviews*, **60**, 261–298.

Alonso-Zarza, A.M. and Arenas, C. (2004) Cenozoic calcretes from the Teruel Graben, Spain: microstructure, stable isotope geochemistry and environmental significance. *Sedimentary Geology*, **167**, 91108.

Arakel, A.V. (1986) Evolution of calcrete in palaeodrainages of the lake Naperby area, Central Australia, *Palaeogeography, Palaeoclimatology, Palaeoecology*, 54, 283–303.

Aristarain, L.F. (1970) Chemical analyses of caliche profiles from the high plains, New Mexico. *Journal of Geology*, **78**, 201–212.

Atabey, E., Atabey, N., and Kara, H. (1998) Sedimentology of caliche (calcrete) occurrences of the Kırşehir region. *Bulletin of the Mineral Research and Exploration*, **120**, 6980.

Atabey, E., Ilgar, A., and Sakitaş, A. (2004) Çanakkale havzasnn Orta-Üst Miyosen stratigrafisi, Çanakkale, KB Türkiye. *Bulletin of Mineral Research and Exploration of Turkey (MTA)*, **128**, 79–97.

Atalay, I. (1996) Paleosols as indicators of climatic changes during Quaternary Period in South Anatolia. *Journal of Arid Environments*, **32**, 23–35.

Bajnoczi, B. and Kovacs-Kis, V. (2006) Origin of pedogenic needle-fiber calcite revealed by micromorphology and stable isotope composition a case study of a Quaternary paleosol. *Chemie der Erde Geochemistry*, **66**, 203212.

Bradley, W.F. (1940) The structure scheme of attapulgite. *American Mineralogist*, **25**, 405–410.

Braithwaite, C.J.R. (1979) Crystal textures of recent fluvial pisolites and laminated crystalline crusts in Dyfed, South Wales. *Journal of Sedimentary Petrology*, **49**, 181–193.

Breitländer (1988) *Pulverproben, Festproben Mineralische, Metallurgische Werkstoffe*. Eichproben und Labormaterial GmbH, Hans-Sachs-Straße 12, D-59077 Hamm, Germany.

Brindley, G.W. (1980) Quantitative X-ray analysis of clays.

Pp. 411–438 in: *Crystal Structures of Clay Minerals and their X-ray Identification* (G.W. Brindley and G. Brown, editors). Monograph **5**, Mineralogical Society, London.

Cerling, T.E. (1984) The stable isotopic composition of modern soil carbonate and its relationship to climate. *Earth and Planetary Science Letters*, **71**, 229240.

Chamley, H. (1989) *Clay Sedimentology*. Springer Verlag, New York, 623 pp.

Christ, C.L., Hathaway, J.C., Hostetler, P.B., and Shepard, A.O. (1969) Palygorskite: new X-ray data. *American Mineralogist*, **54**, 198–205.

Colson, J. and Cojan, I. (1996) Groundwater dolocretes in a lake marginal environment: an alternative model for dolocrete formation in continental settings (Danian of the Provence Basin France), *Sedimentology*, **43**, 175–188.

Çağatay, M.N. (1990) Palygorskite in the Eocene rocks of the Damam dome, Saudi Arabia. *Clays and Clay Minerals*, **38**, 299–307.

Ece, O.I., Coban, F., Gungor, N., and Suner, F. (1999) Clay mineralogy and occurrence of ferrian smectites between serpentinite saprolites and basalts in Biga peninsula, northwest Turkey. *Clays and Clay Minerals*, **47**, 241–251.

Eren, M. (2007) Genesis of tepees in the Quaternary hardpan calcretes, Mersin, S Turkey. *Carbonates and Evaporites*, **22**, 123–134.

Eren, M., Kadir, S., Hatipoğlu, Z., and Gül, M. (2004) Caliche development in Mersin area, TÜBTAK Project, No. 102Y036, 136 pp. (in Turkish with English abstract).

Eren, M., Kadir, S., Hatipoğlu, Z., and Gül, M. (2008) Quaternary calcrete development in the Mersin area, southern Turkey. *Turkish Journal of Earth Sciences*, **17**, 763–784.

Farmer, V. C. (1974) Layer silicates. Pp. 331–363 in: *Infrared Spectra of Minerals* (V.C. Farmer, editor). Monograph **4**, Mineralogical Society, London.

Farmer, V.C. and Palmieri, F. (1975) The characterization of soil minerals by infrared spectroscopy. Pp. 573–671 in: *Soil Components, vol. 2, Inorganic Components* (J.E. Gieseking, editor). Springer-Verlag, New York.

Farmer V.C. and Russell J.D. (1964) The infrared spectra of layer silicates. *Spectrochimica Acta*, **20**, 1149–1173.

Gehring, A.U., Keller, P., Frey, B., and Luster, J. (1995) The occurrence of spherical morphology as evidence for changing conditions during the genesis of a sepiolite deposit. *Clay Minerals*, **30**, 83–86.

Ghazban, F., McNutt, R.H., and Schwarcz, H.P. (1994) Genesis of sediment-hosted Zn-Pb-Ba deposits in the Irankuh district, Esfahan area, west-central Iran. *Economic Geology*, **89**, 1262–1278.

Goudie, A.S. (1972) The chemistry of world calcrete deposits. *Journal of Geology*, **80**, 449–463.

Goudie, A.S. (1973) *Duricrusts in Tropical Landscapes*. Clarendon Press, Oxford, UK.

Goudie, A.S. (1983) Calcrete. Pp. 93131 in: *Chemical Sediments and Geomorphology* (A.S. Goudie, and K. Pye, editors). Academic Press, London.

Goudie, A.S. (1996) Organic agency in calcrete development. *Journal of Arid Environments*, **32**, 103–110.

Gürel, A. (2008) Sedimentological and mineralogical investigation of the Late Miocene successions of Aktoprak Basin (Central Turkey): Implication for sediment source and palaeoclimates. *Clay and Clay Minerals*, **54**, 555–570.

Harrison, R.S. (1977) Caliche profiles: indicators of near-surface subaerial Diagenesis, Barbados, West Indies. *Bulletin of Canadian Petroleum Geology*, **25**, 123–173.

Imai, N., Otsuka, R., and Kashide, H. (1969) Dehydration of palygorskite and sepiolite from the Kuzu District, Tochigi Pref., central Japan. Pp. 99–108 in: *Proceedings, International Clay Conference*, Tokyo.

Inglès, M. and Anadón, P. (1991) Relationship of clay minerals to depositional environment in the non-marine Eocene Pontils Group, SE Ebro basin (Spain). *Journal of Sedimentary Petrology*, **61**, 926–939.

James, N.P. and Choquette, P.W. (1984) Diagenesis 9. Limestones – the meteoric diagenetic environment. *Geoscience Canada*, **11**, 161–194.

Jones, B.F. and Galán, E. (1988) Sepiolite and palygorskite. Pp. 631–374 in: *Hydrous Phyllosilicates (Exclusive of Micas)* (S.W. Bailey, editor). Reviews in Mineralogy, **19**, Mineralogical Society of America, BookCrafters, Inc., Chelsea, Michigan.

Jones, B. and Ng, K.C. (1988) The structure and diagenesis of rhizoliths from Cayman Brac, British West Indies. *Journal of Sedimentary Petrology*, 58, 457–467.

Kadir, S. (2007) Mineralogy, geochemistry and genesis of smectite in Pliocene volcaniclastic rocks of the Doğanbey Formation, Beyşehir basin, Konya, Turkey. *Clays and Clay Minerals*, **55**, 402–422.

Kadir, S. and Eren, M. (2008) The occurrence and genesis of clay minerals associated with Quaternary caliches in the Mersin area, southern Turkey. *Clays and Clay Minerals*, **56**, 244–258.

Kapur, S., Çavuşgil, V.S., and Fitzpatrick, E.A. (1987) Soil-calcrete (caliche) relationship on a Quaternary surface of the Cukurova Region, Adana (Turkey). Pp. 597–603 in: *Soil Micromorphology* (N. Federoff, L.M. Bresson, and M.A. Courty, editors). Association Française pour L'Etude du Sol, Paris.

Kapur, S., Çavuşgil, V.S., Şenol, M., Gürel, N., and Fitzpatrick, E.A. (1990) Geomorphology and pedogenic evolution of Quaternary calcretes in the northern Adana Basin of southern Turkey. *Zeitschrift für Geomorphologie*, **34**, 4959.

Kapur, S., Yaman, S., Gokçen, S.L., and Yetiş, C. (1993) Soil stratigraphy and Quaternary caliche in the Misis area of the Adana Basin, southern Turkey. *Catena*, **20**, 431445.

Kapur, S., Saydam, C., Akça, E., Çavuşgil, V.S., Karaman, C., Atalay, I., and Özsoy, T. (2000) Carbonate pools in soil of the Mediterranean: A case study from Anatolia. Pp. 187–212 in: *Global Climate Change and Pedogenic Carbonates* (R. Lal, J.M. Kimble, H. Eswaran and B.A. Stewart, editors). Lewis Publishers, Boca Raton, Florida, USA.

Khadkikar, A.S. (2005) Elemental composition of calcites in late Quaternary pedogenic calcretes from Gujarat, western India. *Journal of Asian Earth Sciences*, **25**, 893–902.

Khalaf, F.I. (1990) Occurrence of phreatic dolocrete within Tertiary clastic deposits of Kuwait, Arabian Gulf. *Sedimentary Geology*, **68**, 223–239.

Khalaf, F.I. (2007) Occurrences and genesis of calcrete and dolocrete in the Mio-Pleistocene fluviatile sequence in Kuwait, northeast Arabian Peninsula. *Sedimentary Geology*, **199**, 129–139.

Klappa, C.F. (1980) Rhizoliths in terrestrial carbonates: classification, recognition, genesis and significance. *Sedimentology*, **27**, 613–629.

Krekeler, M.P.S., Morton, J., Lepp, J., Tselepis, C.M., Samsonov, M., and Kearns, L.E. (2008) Mineralogical and geochemical investigation of clay-rich mine tailing from a phosphate mine, Bartow Florida, USA. *Environmental Geology*, **55**, 123–147.

Kulbicki, G. (1959) High temperature phases in sepiolite, attapulgite and saponite. *American Mineralogist*, **44**, 752–764.

Land, L.S. (1980) The isotopic and trace-element geochemistry of dolomite: The state of the art. Pp. 87–110 in: *Concept and Models of Dolomitization* (D.H. Zenger and R.L. Ethington, editors). Special Publication No. **128**, Society

of Economic Paleontologists and Mineralogists, Tulsa, Oklahoma, USA.

Mack, G.H., Cole, D.R., Giordano, T.H., Schaal, W.C., and Barcelos, J.H. (1991) Paleoclimatic controls on stable oxygen and carbon isotopes in caliche of the Abo Formation (Permian) South-central New Mexico, U.S.A. *Journal of Sedimentary Petrology*, **61**, 458–472.

Mackenzie, R.C. (1957) *The Differential Thermal Investigation of Clays*. Monograph **2**, Mineralogical Society, London, 456 pp.

MBH Reference Material (1998–99) An ISO 9002 accredited company. 1994 Cert. No. 0524, 99 pp.

McKeown, D.A., Post, J.E., and Etz, E.S. (2002) Vibrational analysis of palygorskite and sepiolite. *Clays and Clay Minerals*, **50**, 667–680.

Moore, D.M. and Reynolds, R.C. (1989) *X-ray Diffraction and the Identification and Analysis of Clay Minerals*. Oxford University Press, New York, 332 pp.

Newman, A.C.D. and Brown, G. (1987) The chemical constitution of clays. Pp. 1–128 in: *Chemistry of Clays and Clay Minerals* (A.C.D. Newman, editor). Monograph **6,** Mineralogical Society, London.

Özer, A.M., Wieser, A., Göksu, H.Y., Müller, P., Regulla, D.F., and Erol, O. (1989) ESR and TL age determination of caliche nodules. *International Journal of Radiation Applications and Instrument. Part A – Applied Radiation and Isotopes*, **40**, 1159–1162.

Paquet, H. (1983) Stability, instability, and significance of attapulgite in the calcrete of Mediterranean and tropical areas with marked dry season. *Sciences Géologique Mémoire*, **72**, 131–140.

Purvis, K. and Wright, V.P. (1991) Calcretes related to phreatophytic vegetation from the Middle Triassic Ottar Sandstone of South West England. *Sedimentology*, **38**, 539–551.

Reeves, C.C., Jr. (1970) Origin, classification, and geologic history of caliche on the Southern High Plains, Texas and Eastern New Mexico. *Journal of Geology*, **78**, 352362.

Roger, L.E.R., Martin, A.E., and Norrish, K. (1964) The occurrence of palygorskite, near Ipswich, Queensland. *Mineralogical Magazine*, **30**, 131–158.

Sancho, C., Melendez, A., Signes, M., and Bastida, J. (1992) Chemical and mineralogical characteristics of Pleistocene caliche deposits from the central Ebro Basin, NE Spain. *Clay Minerals*, **27**, 293–308.

Schmid, S., Worden, R.H., and Fisher, Q.J. (2006) Sedimentary facies and the context of dolocrete in the Lower Triassic Sherwood Sandstone group: Corrib Field west of Ireland. *Sedimentary Geology*, 187, 205–227.

Serratosa, J.M. (1962) Dehydration and rehydration studies of clay minerals by infrared absorption spectra. *Proceedings of the 9th National Conference on Clays and Clay Minerals*, Pergamon Press, New York, 412–418.

Singer, A. (1979) Palygorskite in sediments: detrital, diagenetic, or neoformed – a critical review. *Geologische Rundschau*, **68**, 996–1008.

Singer, A. (1984) Pedogenic palygorskite in the arid environment. Pp. 169–176 in: *Palygorskite-sepiolite Occurrence, Genesis and Uses* (A. Singer and E. Galán, editors). Developments in Sedimentology, **37**, Elsevier, Amsterdam.

Singer, A. (1989) Palygorskite and sepiolite group minerals. Pp. 829–872 in: *Minerals in Soil Environments* (J.B. Dixon and S.B. Weed, editors). Soil Science Society of America, Inc., Madison, Wisconsin, USA.

Smykatz-Kloss, W. (1974) *Differential Thermal Analysis, Application and Results in Mineralogy*. Springer-Verlag, Berlin, 185 pp.

Suchecki, R.K., Hubert, J.F., and Birney De Wet, C.C. (1988) Isotopic imprint of climate and hydrogeochemistry on terrestrial strata of the Triassic-Jurassic Hartford and Fundy rift basins. *Journal of Sedimentary Petrology*, **58**, 801–811.

Van der Marel, H.W. and Beutelspacher, H. (1976) *Atlas of IR Spectroscopy of Clay Minerals and their Admixtures*. Elsevier, Amsterdam, 396 pp.

Velde, B. (1977) *Clays and Clay Minerals in Natural and Synthesic Systems*. Elsevier/North-Holland Inc., New York, 218 pp.

Verrecchia, E.P. and Coustumer, M.L. (1996) Occurrence and genesis of palygorskite and associated clay minerals in Pleistocene calcrete complex, SDE Boqer, Negev Desert, Israel. *Clay Minerals*, **31**, 183–202.

Webb, T.L. and Krüger, J.E. (1970) Carbonate. Pp. 303–341 in: *Differential Thermal Analysis, volume 1, Fundamental Aspects* (R.C. Mackenzie, editor). Academic Press, London and New York.

Wright, V.P. (1986) The role of fungal biomineralization in the formation of Early carboniferous soil fabrics. *Sedimentology*, **33**, 831–838.

Wright, V.P. and Tucker, M.E. (1991) *Calcretes*. The International Association of Sedimentologists in association with Blackwell Scientific Publications, Oxford, London, 352 pp.

Wright, V.P., Platt, N.H., and Wimbledon, W.A. (1988) Biogenic laminar calcretes: evidence of calcified root-mat horizons in paleosols. *Sedimentology*, **35**, 603–620.

(*Received 9 March 2009; revised 13 November 2009; Ms. 292; A.E. H. Dong*)